Fluid-particle Correlated Motion and Turbulent Energy Transfer in a Two-dimensional Particle-laden Shear Flow

S. Horender

Zentrum für Ingenieurwissenschaften

Martin- Luther Universität Halle-Wittenberg, 06099 Halle(Saale), Germany,

stefan.horender@iw.uni-halle.de, s.horender@web.de

Y. Hardalupas

Mechanical Engineering Department,

Imperial College, Exhibition Road, London SW7 2BX, UK,

tel. +44-20-7594705, fax +44-20-75941472

y.hardalupas@imperial.ac.uk

published in Chem. Eng. Sci. 65 (2010) 5075–5091

Abstract

Discrete Vortex Simulations of a dilute two-dimensional particle-laden shear layer with one-way coupling were performed to study fluid-particle correlated motion and the transfer of turbulent kinetic energy between the phases. The resulting modification of carrier phase turbulence, estimated according to current computational models, was evaluated. Particle Stokes numbers were between 1.0 and 4.5, so that the particles showed considerable temporal concentration fluctuations due to centrifuging by the fluid flow structures, and the mass loading was 12% corresponding to a volume fraction of $6.0 \cdot 10^{-5}$.

Fluid velocities and particle concentration and velocities and their covariances, which appear in a commonly used model equation for carrier phase turbulence modification, were evaluated. Additionally, the probability density functions of fluid velocity fluctuations viewed by the particles are presented and compared with their Eulerian counterparts. It was found that particles view reduced velocity fluctuations due to preferential clustering. The model for carrier-phase turbulence

modification predicted turbulence reduction, depending on the particle Stokes number. The mechanism responsible for turbulence reduction was the correlated velocity fluctuations of fluid and particles and this reduction could reach values up to one third of the fluid flow dissipation. Preferential particle concentration together with a relative velocity between the phases could generate turbulent kinetic energy of the gas phase, however this production was nearly an order of magnitude smaller compared to reduction of turbulence due to the correlated motion. The findings were compared with experiments available in the literature and help to clarify the view when turbulence reduction or augmentation occurs.

Keywords: Turbulence; Turbulence Modification; Transport Processes; Fluid-particle correlated motion; Fluid Mechanics; Multiphase Flow

1. Introduction

Prediction of turbulence levels of the continuous phase in two phase flows is important for modelling dispersion of solid particles or droplets, particle collisions or mixing of gaseous species. The modification of carrier turbulence levels may have important consequences on the desired performance of technical processes. For example, Horender et al. (2008) modelled the outside vapour deposition process for the production of ultra pure glass for optical fibres and found that turbulence is, besides thermophoresis, the most important deposition mechanism. Hence, for an exact prediction of deposition efficiencies, which contribute considerably to the commercial success of such a process, the influence of the particle mass loading on the turbulence structure of the carrier gas has to be modelled adequately. However, full understanding of the mechanisms of fluid turbulence modification due to the presence of particles has not been achieved, although numerous studies have been carried out.

Reviews on experiments focussing on turbulence modification in flows laden with particles or bubbles can be found in Hetsroni (1989) or Gore & Crowe (1991). They concluded that the ratio of particle diameter to flow length scale could describe qualitatively the trends of turbulence modification. For flows in which this ratio was below 0.1, turbulence reduction was found, while for larger values turbulence enhancement was experienced. However, the proposed conclusion from the above reviews was independent of the particle mass loading in the corresponding flows, which is a quantity that is expected to influence the continuous phase behaviour in the presence of particles. More recently additional experiments and simulations were carried out. Sckreck & Kleis (1993) studied experimentally the modification of grid-generated turbulence in a water flow using particles with a diameter of approximately 5 times the Kolmogorov scale. They also found an increased isotropy of the velocity fluctuations of the water flow and from that concluded that the presence of the particles modifies the dynamics of the fluid turbulence, not only by exchange of momentum and energy, but also due to a possible influence of the particles on the flow structure. Kulick et al. (1994) measured turbulence modification by 50 and 90 μm glass beads and 70 μm copper particles in a pipe flow and found that the copper particles reduced the carrier phase turbulence levels while the glass beads had little effect. Fessler & Eaton (1999) performed similar measurements in a backward facing step and found that turbulence reduction was a function of particle Stokes and Reynolds number and the specific flow regime. Both experimental studies will be discussed in more detail in the results section. Hädrich (2001) measured gas velocity spectra in a particle-laden channel flow with LDA technique and found that small and larger particles (compared to the eddy size) decreased the energy at large frequencies. The small particles reduced

energy also at the smaller frequencies, corresponding to the large vortices in the flow, which, however, were not affected by the larger particles. Kussin & Sommerfeld (2002) performed experiments in a narrow particle-laden channel flow and measured turbulence modification of the carrier gas as function of particle size and wall roughness. They found that particles smaller than 200 μm reduced the gas phase turbulence and that an increased wall roughness led to increased turbulence attenuation by the particles. Larger particles augmented turbulence in the core of the channel and reduced it in the near-wall regions. This trend of turbulence modification confirmed the conclusions of Gore & Crowe (1989).

Hagiwara et al. (2002) conducted simultaneous visualisation of depositing copper particles and fluorescent tracers in a turbulent water flow in a horizontal duct. They found that the rms of streamwise velocity fluctuations was decreased by vertically elongated clusters in the shear region close to the wall. Ljus et al. (2002) preformed measurements of turbulence modification of the air flow laden with spherical particles and pulp fibres at mass loadings 0.03 and 0.1 in a Venturi tube connected to a horizontal pipe. The measurements showed that the turbulence intensities increased close to the centre of the pipe, while they decreased close to the wall for the spherical particles. The fibres decreased the turbulence over the entire pipe cross-section, however changed the mean velocity profile, which gave rise to turbulence production in the lower part of the pipe. Geiss et al. (2004) investigated grid generated turbulence modification in a downward air flow laden with glass beads of sizes 120, 240 and 480 μm, which were fed to the gas flow upstream of the turbulence generating grid. Measurements were taken with a two-component PDA system. The particles showed larger velocity fluctuations than the gas phase and they observed that the smaller particles attenuated and the larger particles augmented carrier phase turbulence and that all particles induced anisotropic velocity fluctuations of the gas. For the larger particles they were able to draw the clear conclusion that the wakes are responsible for turbulence enhancement. However they suggested that the physics for 120 μm particles are more complex and a counter-balance between extra dissipation and production may exist. This view was justified by the authors due to the fact that the smaller particles changed the initial conditions of gas turbulence (as did the larger ones), however the decay of turbulence was similar for the clean flow and the flow laden with the smallest particles. In contrast to that the decay was smaller for the flow laden with largest particles.

More recently, Yang & Shy (2005) investigated counter-rotating fan generated turbulence in an air flow with settling particles and observed turbulence augmentation, although the particle sizes were equal or smaller by approximately a factor of two compared to the Kolmogorov scale. Additionally, they found an increased settling rate due to particle-turbulence interaction, when compared to the

still air terminal velocity of particles. They suggested that this increase was caused by preferential particle concentration which aligned with the flow vortices and led to turbulence augmentation. Hwang & Eaton (2006) conducted experiments in air with heavy particles falling through a box of nearly isotropic and homogeneous turbulence with mass loadings up to 0.3. They found that the particles damped air turbulence up to 40% and the dissipation rate up to 50%. It should be noted that they could not directly measure the dissipation rate due to the resolution of the PIV technique, hence used an LES analogy to estimate the energy flux through the inertial subrange. They could not explain the magnitude of dissipation due to the presence of particles by the standard model, which will be introduced below in eq. (1). Additionally, Hwang & Eaton (2006) reviewed several direct numerical simulation studies and found that these also under-predicted turbulence attenuation. They argued that the particles may have stronger influence on the air turbulence, since the particle diameters of 160 μm were very close to the Kolmogorov length scale and hence the assumption, always used in calculations, that the particles are represented as 'points' (do not occupy any volume) moving according to a drag law, may not be valid. Additionally, they observed that the carrier fluid turbulence became non-isotropic, since the energy spectra of the horizontal fluid velocity fluctuations decreased in a uniform way over all measurable wave numbers. However, the vertical component showed similar level at low wave numbers, but the amount of attenuation decreased at higher wave numbers. Poelma et al. (2007) conducted experiments in a particle-laden grid generated turbulent upward water flow at mass loadings 0.1 to 1.0% and corresponding volume loadings of 0.08 to 0.4%. The particles had different densities and sizes of the order of the Kolmogorov scale. They found that the particles shifted the onset of turbulence decay downstream and the particles enhanced the fluid turbulence due to wake production after sufficient decay of the turbulent velocity fluctuations further away from the grid. The flow increased its anisotropy leading to larger fluid velocity fluctuations for the streamwise compared to the cross-stream component. This opposes the finding of Schreck & Kleis (1993), although the flows were the same, and a possible reason could be the different ratio of particle diameters to Kolmogorov scale.

Bini & Jones (2008) performed large eddy simulations of a droplet-laden mixing layer and studied turbulence modification of the carrier fluid. The droplets were smaller than the Kolmogorov scale and the point particle approximation should be valid. Due to the coherent nature of the mixing layer the droplets showed considerable concentration fluctuations. They observed that few large scale frequencies of the carrier gas gained energy while the remaining modes were attenuated. Ten Cate et al. (2004) used a Lattice Boltzmann Method to simulate fully resolved spheres in isotropic turbulence with the particle size approximately ¼ of the Kolmogorov length scale. They found that

on the particle surface and in the wakes additional dissipation occurred, which led to a reduction of large scale turbulent energy due to the energy cascade.

Although the above work has studied the effect of mean particle concentration on carrier phase turbulence modification, little information is available on the influence of concentration fluctuations. Direct numerical simulations in isotropic turbulence were performed, e.g. Boivin et al. (1998), who studied turbulence modification, but they argued that the influence of particle concentration fluctuations was negligible, since their flow did not show coherent fluid structures. Vermorel et al. (2003) used direct numerical simulation to calculate a particle-laden 'slab' flow and found turbulence reduction in the centre of the 'slab' and turbulence enhancement at the edges, see their figures 13 and 18. The enhancement was attributed to turbulence production due to enhanced gas mean velocity gradients and a strong relative velocity between the phases combined with a large correlation of particle distribution and gas velocity fluctuations.

While wake effects of the particles on the carrier fluid seem to be difficult to model, it is straight forward to model the extra dissipation of particles based on the correlation of the fluid velocity fluctuations with the force due to the particles. Hence, the goal of this work is to study numerically the absolute and relative magnitudes of all terms appearing in the commonly used model equation for carrier phase turbulence modification as derived by Elghobashi & Abou-Arab (1983) or Chen & Wood (1985) and used by, e.g., Kulick et al. (1994) for the case that drag is the only relevant force on the particles:

$$\frac{dk}{dt} = \frac{\partial k}{\partial t} + U_i \frac{\partial k}{\partial x_i} = \left(\frac{dk}{dt}\right)_{sp} + \Pi_k \tag{1}$$

$$\Pi_k = -\frac{C}{\rho_f \tau_p}\left(\left\langle u'_{if} u'_{if}\right\rangle - \left\langle u'_{if} u'_{ip}\right\rangle\right) - \frac{1}{\rho_f \tau_p}\left(\left\langle c' u'_{if} u'_{if}\right\rangle - \left\langle c' u'_{if} u'_{ip}\right\rangle\right) - \frac{1}{\rho_f \tau_p}\left(U_{if} - U_{ip}\right)\left\langle c' u'_{if}\right\rangle$$

term 1 *term 2* *term 3*

Here, <...> denotes time averaging, hence the covariance of the involved quantities and capital letters are time averaged quantities. For time dependent variables after subtraction of the corresponding mean values, dashed small letters are used. C is the particle concentration and u_f and u_p are the fluid and particle velocities, respectively. The index i denotes the axis of the cartesian co-ordinate system and the sum is taken over i. As a simplification, the drag force is described using only the particle relaxation time assuming Stokes drag and the slip velocity, hence neglecting the dependence of the Reynolds number on the drag coefficient. The quantity C/ρ_f is the local mass loading of particles in the fluid flow. In the following text dealing with a two-dimensional shear

flow, the streamwise velocity component will be denoted with *u* and the cross-stream component with *v*. Eq. (1) contains covariances of fluctuating quantities rather than correlations, which are covariances normalised by the rms of contributing values.

For the derivation of eq. (1), Chen & Wood (1985) assumed that the governing equations for the fluid and particle phase, hence in an Eulerian-Eulerian description, appear at every point in the flow. Hence, the averaging operator <…> is defined straight forward. For a Lagrangian description of the particle phase, Vermorel et al. (2003) - eq. 10 - used the conditional average defined at the particle positions:

$$\left\langle \Phi \right\rangle_p (x,t) = \frac{\sum_{n=1}^{N_p} \Phi \delta(\vec{x} - \vec{x}_p)}{N_p} \tag{2}$$

Here, Φ is an arbitrary quantity and δ the delta function which is one at the particle position. All particles are assumed to have equal mass and N_p is the number of particles contributing to the average. Based on that averaging they derived the source term for the turbulent kinetic energy of the carrier phase as:

$$\Pi_k = -\frac{C}{\rho_f \tau_p}\left(\left\langle u'_{if} u'_{if} \right\rangle_p - \left\langle u'_{if} u'_{ip} \right\rangle_p\right) + \frac{C}{\rho_f \tau_p}\left\langle u_{ip} - u_{if} \right\rangle_p \cdot \left\langle u'_{if} \right\rangle_p \tag{3}$$

term 1a *term 2a*

where the operator $<\ldots>_p$ represents averaged quantities as seen by particles. Simonin et al. (1993) explained that the term $<u'_f>_p$ is equal to $<c'u'_f>$ in the limit that the particles behave as tracers and perfectly follow the flow. Hence, what is expressed as particle concentration fluctuation in eq. (1) is here contained in the conditional averaging of the flow variables. In the literature, $<u_{ip}\text{-}u_{if}>_p$ is also referred to as the relative velocity U_{ir}, and $<u'_{if}>_p = <u_f\text{-}U_f>_p$ is often denoted as drift velocity U_{id}, see Simonin et al. (1993), with

$$U_{id} = U_{ip} - U_{if} - U_{ir} \tag{4}$$

.

This formulation is mathematically more general and is also applicable when particles are not present at all positions in vortex dominated disperse phase flows, as can be observed in fig. 1. Hence, eq. (3) will be used to evaluate turbulence modification of the gas phase by particles in this work.

Usually, only the contribution of *term 1* or *term 1a* of eq. (1) or (3) respectively on turbulence modification is considered, while the other terms are assumed to be negligible. Kulick et al. (1994) - p. 129 - pointed out that very little is known about the relative magnitude of the contained terms,

hence they will be evaluated for a simple shear flow in this work. Only few measurements of the average of the fluid velocity seen by the particles are reported in the literature, see for example Hardalupas & Horender (2003b), who estimated this quantity using PDA technique in a spray, and references therein.

It should be noted that the covariances are an average over all scales of the fluid velocity fluctuations. Additionally, the model assumptions take into account only a pure statistical description of the turbulent fluctuations in the flow rather than the real interacting vortices with an energy cascade. Hence, the effect that Hädrich (2001) points out, that particles may partially follow the energy containing eddies in a turbulent flow and thereby 'consume' their energy, is included in the model. What is missing in the model is the yet unknown effect due to these vortical structures and their interplay with the particles. Therefore the model is only valid for dilute disperse phase flows, where the effect of the particles on the flow scales linearly with their concentration. Hence, the simulations in this work will use one-way coupling and evaluate the indirect effects of eqs. (1) and (3). Also wake effects or streamline distortion are not considered in this model. Some experimental work used eq. (1) to explain the magnitude of the observed carrier phase turbulence reduction. For example, Hwang & Eaton (2006) - p. 390 - found that this model could only account for one third of the measured turbulence reduction. (Here it should be noted that there may be a small error in their simplified evaluation of extra dissipation, since they considered only one velocity component in the three-dimensional flow.) They argued that this far too small prediction may be due to the highly unsteady near field of the particle and that the Basset and the history force may have significant contributions on the particle drag, which was neglected. They did correct the particle relaxation time based on the Reynolds number dependent drag coefficient, however used the free fall velocity for that correction. Further improvements and their consequences will be investigated in the results section of this work. Also, Schreck & Kleis (1993) found that such a simple model predicted too low extra dissipation. Hence, the models of eqs. (1) and (3) may be incomplete for the description of extra dissipation due to the presence of particles as stated above and may only describe a part of the truth. Other mechanisms may be also relevant but have not been generally identified. Nevertheless, there is a need to evaluate these models, since it may be possible to describe some of the trends in measured turbulence modification as will be presented in the discussion section.

The physical interpretation of *terms 1, 2 and 3* of eq. (1) will be presented in the following section and their magnitude will be evaluated to decide the relative importance of all terms for a computer generated particle-laden shear layer flow. A shear layer flow was chosen for the desired evaluation,

since it comprises a comparatively simple flow structure, which is well understood for the fluid and the particle flow and some of the work on this type of flow is summarised as follows. Early work used hot-wire anemometry to characterise the fluid flow in shear layers, e.g. Wygnanski & Fiedler (1970), who presented mean and rms velocity data and higher order correlations and consequent estimates of the energy balances in the flow. Brown & Roshko (1974) produced shadowgraphic images of planar mixing layers between different gases and Winant & Browand (1974) performed experiments with dye visualisation of a mixing layer in water. Both investigations indicated the existence of two-dimensional organised structures.

Crowe et al. (1985) were the first to identify the large scale vortex pairing structure as dominating effects for particle dispersion in shear flows. They scaled previous experiments using a Stokes number, defined as the ratio of particle relaxation time τ_p and time scale of the fluid vortices τ_f. They found that for Stokes number around unity, particles or droplets become entrained in the large-scale structure and may be centrifuged at the outer edges of the structures.

After that, numerous work has been published on two-phase shear flows. Wen et al. (1992) investigated experimentally and numerically a two-phase shear flow and presented fluid and particle velocities without considering particle concentration fluctuations. Chang et al. (1993) presented measurements of droplet mean streamwise and cross-stream velocities in a downward air shear flow laden with a water spray with a size range 3 to 100 μm. They used a finite volume method to predict the air flow and a stochastic tracking of individual droplets, and found reasonable agreement with the experiments; however, they predicted too small cross-stream droplet velocities. Hishida et al. (1992) measured mean and rms streamwise and cross-stream velocities of both phases including the shear stresses using laser Doppler anemometry. They estimated particle dispersion in cross-stream direction and found maximum dispersion for Stokes numbers around unity. Lázaro & Lasheras (1992) used imaging and laser diffraction sizing techniques to measure the Sauter mean diameter (SMD), the mean particle concentration and the spreading rate in a spray-laden horizontal shear layer, with the low speed side on the upper side of the flow. They also passed a laser beam along the spanwise direction through the shear layer flow and used light absorption to measure droplet concentration fluctuations. The cross-correlation of droplet concentration and fluid velocity showed that the locations where the droplets were clustered and centrifuged to the low speed side of the shear layer corresponded to the regions between successive vortices. Hardalupas & Horender (2003a) presented measurements of the velocity and concentration characteristics of a particle-laden shear flow and also used a discrete vortex method (DVM) to simulate the flow and found reasonable agreement for particle velocities and turbulent particle mass flux. In other shear

dominated flows particle centrifuging was also found. For example Longmire & Eaton (1992) used phase-locked digital imaging to measure the spatial distribution of particle number density in a pulsed jet laden with glass beads. They found that the instantaneous number density, integrated radially over the jet, had maximum values up to three times larger than the minimum values. Therefore, it is obvious that large particle concentration fluctuations are present in such flows.

DVM was selected here to simulate the particle-laden shear layer flow, since it is comparatively simple to implement for two dimensional turbulent shear flows and is well described in the literature. Chorin (1973) reinvented the method by using vortex blobs and Leonard (1980, 1985) and Sarpkaya (1989) compiled reviews of the method and a more mathematical treatment can be found in Cottet & Koumoutsakos (2000). Chung & Troutt (1988) simulated particle dispersion in an axisymmetric jet and found good agreement with experiments for the ratio of dispersion of particles and fluid elements for different Stokes numbers. Chein & Chung (1988) simulated a particle-laden mixing layer with DVM and also found dispersion of particles beyond the boundaries of fluid elements for Stokes numbers around unity. Particles introduced to the flow from the low speed side showed larger dispersion and mixing than particles released from the high speed side due to larger local interaction times on the low speed side. Uchiyama & Naruse (2006) modelled chemical reaction of two passive scalars in a two-dimensional mixing layer using DVM. They found that the mixing due to large scale coherent vortices was captured well and the resulting concentration profiles agreed well with finite difference analyses from the literature. Huang et al. (2006) used DVM to calculate particle dispersion in the wake of a cylinder for Stokes (St) numbers 0.01 to 1000. They found that dispersion was a monotonic function of St and larger particles diffused less. For St between 0.1 and 10, the calculations showed that particles which were on one side of the cylinder wake could cross the centre line and diffuse to the symmetrical side of the flow and further (up to radial distances of 2 cylinder diameters) due to interaction with fluid vortices. Direct numerical simulation was used by Ling et al. (1998) to study three-dimensional dispersion in a particle-laden shear layer. Summaries of related experimental and numerical work can be found in Crowe et al. (1993) or Eaton & Fessler (1994), who focussed also on preferential particle concentration.

The main purpose of the current contribution is to use DVM to calculate all the terms of eq. (3) in a shear layer particle-laden flow and to compare their contributions to the total resulting turbulence modification of the fluid flow. One-way coupling was considered, which is commonly used in LES and DNS calculations; hence the influence of particle phase on the fluid flow was neglected. Therefore, the effect of the particle-fluid correlated motion on modelling turbulence modification

can be evaluated directly without the effect on mean carrier-fluid gradients and its consequences on turbulence.

The manuscript first presents an interpretation of the physical interactions between the two phases described by the model of eqs. (1) and (3). Then, the numerical technique, particle tracking and data processing are described. The characteristics of the fluid and particle phases are presented and the resulting turbulence modification is discussed with respect to experimental findings and theoretical considerations in the literature. The paper ends with a summary.

2. Physical interpretation of the model equation

This section presents an interpretation of possible flow structures which can be responsible for turbulence modification of the carrier phase by the presence of particles as described by eqs. (1) and (3). Therefore, the three terms are discussed separately in the order of appearance. It should be noted that the terms contained in eq. (1) are used for that description, since they are easier to understand due to the fact that only Eulerian time averages need to be considered. It should be noted that Vermorel et al. (2003) presented a valuable analysis of eq. (3) and showed that the interphase transfer due to particle agitation can be expressed as the sum of wake production and turbulent transfer. In the current work, the focus will be on the turbulent energy transfer with the mechanism described below.

It should be noted here that this model assumes that the fluid has stochastically independent velocity fluctuations and completely neglects the (vortical) structure of a turbulent fluid flow. This could partly contribute to the inaccuracies of the model to describe measured turbulence modification as described in the introduction.

Term 1: This term contains the covariance of fluid and particle velocities, also known as ‘fluid velocity seen by the particles’. This quantity is the average instantaneous slip velocity, which is different from the mean slip velocity, if the particles are not perfectly responsive to the fluid flow velocity fluctuations. The physical meaning of *term 1* is related to the transfer of turbulent kinetic energy and momentum between the particles and the fluid. If the velocity fluctuations of the fluid and particles were equal and perfectly correlated, the transfer of kinetic energy from the particles to the fluid would be zero, since there would be no instantaneous slip velocity, hence no drag force. Consequently, *term 1* would be zero for that case. If the fluid and particle velocities were uncorrelated with a fluid-particle velocity covariance of zero, the reduction of turbulent kinetic energy of the carrier phase would be maximum, since there is great chance that a particle with high

velocity is surrounded by fluid with small velocity and vice versa. Hence, for that combination, the instantaneous slip velocity is maximised and so does the energy transfer, leading to carrier phase turbulence reduction.

Another possibility would be that the particle velocity fluctuations are larger than that of the fluid and are well correlated with the fluid flow. That could lead to enhancement of carrier phase turbulence and this would describe a flow where the particles dominate the fluid flow velocity fluctuations. Particles with velocity larger than the corresponding average coincide with fluid with large velocity and the fluid velocity is increased even further and vice versa for lower than average velocities. Elghobashi and Truesdell (1993) observed this behaviour in DNS calculations of decaying turbulence after the turbulent kinetic energy of the fluid had fallen below that of the particles.

Term 2: In general, this term has the same structure as *term 1*, containing the fluid-particle velocity covariance. This means that the term describes the balance of energy and momentum between the particle and fluid phase not only in terms of fluctuating velocities, but also includes the fluctuating particle concentration. Following the discussion for *term 1*, not only the instantaneous slip velocity governs the transfer of energy and momentum, but also the local concentration, hence the instantaneous local mass loading of particles. For eq. (3) both *terms 1 and 2* are included in *term 1a* due to the conditional averaging.

Term 3: In the literature, the physics of the covariance of particle concentration and fluid velocity fluctuations in relation to carrier phase turbulence modification has not been discussed, although models for these quantities have been developed, e.g. Reeks (1993). *Term 3* also describes the influence of an unsteady mass loading on the transfer of kinetic energy. Assume a flow laden with particles, which have all the same velocity, hence the rms of particle velocity fluctuations is zero. Additionally, the fluid flow velocity fluctuates around a mean value and the particle concentration fluctuations are correlated with the fluid velocity fluctuations so that large particle concentration coincides with high instantaneous fluid velocity, so $\langle c' u'_f \rangle$ is not zero. If there is a slip velocity between the two phases and the particles are faster than the fluid, there is a drag between the phases, hence energy and momentum are transferred. At positions where the particle concentration is high, more energy is transferred compared to a location with small particle concentration. Since, in this hypothetical flow, high particle concentration is correlated with high fluid velocity and the particles are faster than the fluid, the fluid velocity will be increased. However, at a location in the flow, where the fluid velocity is small, also the particle concentration is small, hence the fluid velocity is increased less due to particle drag. Consequently, the rms of fluid velocity fluctuations is increased.

This behaviour of the hypothetical flow is predicted by eq. (1), since $<c'u'_f>$ was positive and the fluid mean velocity was smaller than the particle velocity. The 'minus' sign in front of this term makes its contribution to the modification of carrier phase turbulence positive. Now, consider that a particle would have been slower than the fluid phase. This would mean that at locations with high particle concentration the fluid velocity is decreased, but by a larger amount compared to locations where fluid velocity and particle concentration are low. Hence, the fluid rms velocity is decreased. It should be noted that the same argument can be used for negative $<c'u'_f>$. An enhancement of carrier fluid turbulence was found in DNS calculations of Vermorel et al. (2003) at the edges of a particle-laden slab flow. *Term 2a* describes exactly the same mechanism, however it has also the advantage that it is defined for regions in the flow with and without particles.

In summary, *term 1* reduces fluid turbulence, except for cases of particle velocity fluctuations larger than those of the fluid and well correlated to each other, when it enhances fluid turbulence. *Term 2* describes the same mechanism and the same effects as term 1, but also includes the influence of particle concentration fluctuations. *Term 3* describes carrier phase turbulence enhancement as well as reduction, depending on the sign of the slip velocity and of the covariance of particle concentration and fluid velocity. Therefore, there are cases that all terms can either enhance or reduce fluid turbulence depending on flow conditions.

The total outcomes of eqs. (1) or (3) depend on $1/\tau_p$ and the difference in velocity covariance of the fluid seen by particles and fluid-particle covariance. These two quantities have opposing trends, since lighter and/or smaller particles follow better the fluid velocity fluctuations, hence have larger fluid-particle velocity covariance, which is subtracted from the viewed fluid auto-covariance. This auto-covariance also depends on the particle relaxation time, as will be seen later, which makes the overall contribution complex. The resulting trends are discussed for two particle sizes in this manuscript. Additionally, τ_p is a function of the instantaneous slip velocity due to the Reynolds number dependence on the drag coefficient. For example, Hwang & Eaton (2006) introduced a correction of the particle relaxation time based on the Schiller & Naumann correlation for the drag coefficient of a sphere, which will be explained in the section on the numeric technique, as:

$$\tau_{p,c} = \frac{\tau_p}{1 + 0.15\,\mathrm{Re}_p^{0.687}} \tag{5}$$

It is not clear, in the current flow, whether enhancement or reduction of carrier phase turbulence is possible, depending on the flow conditions. Consequently, with all covariances in eq. (3) available from calculations, the magnitude of all terms can be evaluated and the transfer of turbulent kinetic energy derived.

3. Simulation technique

3.1 Fluid flow

A computer program based on the discrete vortex method was developed to calculate the shear layer flow. The mathematical basis of the method is to satisfy the non-viscous vorticity transport equation

$$\frac{D\omega}{Dt} = 0 \tag{6}$$

by tracking vortices to compute instantaneously the fluid development in a free shear layer flow. The vortex blob method was used, as reviewed by Leonard (1980) or Sarpkaya (1989), which avoids singularities for the case that vortices approach each other leading to infinitely large velocities. The equations describing the velocities read as follows:

$$u(x,y) = \left(-\frac{1}{2\pi} \sum_{i=1}^{N} \Gamma \frac{y - y_i}{\left|\vec{r} - \vec{r}_i\right|^2 + b^2} \right) + u_{convect} \tag{7}$$

$$v(x,y) = \frac{1}{2\pi} \sum_{i=1}^{N} \Gamma \frac{x - x_i}{\left|\vec{r} - \vec{r}_i\right|^2 + b^2} \tag{8}$$

$r=(x,y)$ is the 2-dimensional location and the velocity vector is (u,v) and i is the index counting the vortices. The constant factor b in the denominator is referred to as vortex blob size in the literature and represents a numerical fluid viscosity without dissipating energy. b was set to 0.35 times the initial distance of vortices located at the splitter plate following initial tests. This ratio is in agreement with Chung & Troutt (1988). The inflow boundary conditions for the generation of a free shear flow were satisfied by adding vortices on the virtual splitter plate with an initial distance of 1.75 mm and releasing them at the end of the plate. As a consequence, the absolute value of the vortex blob size b was then 0.35*1.75 mm=0.61mm.

The vortex strength Γ was set according to a velocity difference between the two streams of the shear layer of 5 m/s and $u_{convect}$ was 3.5 m/s, according to experiments by Hardalupas & Horender (2003a). The outflow boundary conditions were satisfied in a similar way as the inflow, by adding vortices at y = 0 along the direction of the flow at locations larger than the region of interest, which was x = 800 mm in the presented results. The equations were solved for 3.0 s with a time step of 0.25 ms and the first 0.3 s of the flow computation were not used for the processing, since this time was needed for the flow to develop. After that time all initially placed vortices had left the flow domain. Figure 1 shows the basic flow structure of the computational vortices and the co-ordinate system.

The length scale of the dissipative structures was estimated to be equal to the vortex blob size, which is around 610 μm. Since the particles were smaller than those dissipative structures, particle wakes would hardly influence the fluid flow and dissipate quickly. The commonly estimated Kolmogorov length scale η is usually only a fraction of the size of the dissipative motions, see for example Pope (2000, p. 347). From the discussion presented there it is evident that the Kolmogorov length scale is one order of magnitude smaller than the size of the dissipative scales. This ratio is in agreement with the estimation of the Kolmogorov scale in the experimental shear flow of 68 μm presented in Horender & Hardalupas (2009). This estimate was based on the Taylor micro scale derived from the measured velocity autocorrelation function, therefore is not expected to be very accurate. Although, it would allow to derive the dissipation rate according to

$$\eta = \left(\frac{\nu^3}{\varepsilon} \right)^{\frac{1}{4}} \tag{9}$$

and, consequently, it would be possible to compare it to the extra dissipation due to the presence of the particles. However, already small errors in the estimation of the Kolmogorov length scale would lead to large errors in the dissipation rate, since it scales with the power of four. Therefore, we decided to give a value for the dissipation rate in the shear flow based on the CFD simulations of Melheim et al. (2005), which used a k-ε turbulence model to predict the real flow of Hardalupas & Horender (2003a). The dissipation rate was predicted approximately 15 m^2/s^3 on the centre line at streamwise position 300 mm, which corresponds to a Kolmogorov scale of 110 μm in eq. (9).

3.2 Particle flow

The particles were injected at the end of the virtual splitter plate at position x=0 and y=0. For both particle sizes the injection velocity was 3.5 m/s in the streamwise direction and 0 m/s for cross-stream component, so that no slip velocity between the particles and the fluid was present at the inlet position. No velocity fluctuations were applied. Two particle sizes were used, corresponding to 55 and 90 μm glass beads with particle relaxation times of 21 and 58 ms, respectively, and the mass loading was assumed to be 12% according to experiments by Hardalupas & Horender (2003a). This corresponds to a volume fraction of $6.0 \cdot 10^{-5}$ and for that value inter particle collisions are not important and, hence, have not been considered in the calculations.

The Stokes numbers, *St*, defined as the ratio of particle relaxation time to the large eddy time scale, changed with streamwise position of the flow, since the vortical structures grow with downstream

development. For the smaller particles, *St* was 1.7, 1.2 and 1.0 for streamwise positions *x*=200, 300 and 400 mm and, for the larger particles, St was 4.5, 3.2 and 2.6 at these positions, respectively. The particle Reynolds number was between 4 and 7, assuming air properties for the carrier fluid and a slip velocity of 1 m/s.

Gravity was set to zero or 9.81 m/s and the particles were tracked through the flow due to drag with the equation of motion of the particles using the Schiller and Naumann correlation, as used by Ling et al. (1998):

$$\frac{d\vec{U}_p}{dt} = \frac{3\rho_f}{4\rho_p d_p}\frac{24}{\mathrm{Re}_p}\left(1+0.15\,\mathrm{Re}_p^{0.687}\right)\cdot\left(\vec{U}_p-\vec{U}_f\right)\left|\vec{U}_p-\vec{U}_f\right|+\vec{g} \tag{10}$$

Here, ρ denotes the fluid and particle densities, respectively, and Re_p is the particle Reynolds number based on its diameter and the slip velocity. It should be noted that the term in the first bracket on the right hand side corresponds to the correction of the particle relaxation time as introduced in eq. (5). The velocity and position of each particle were derived by integrating the equation of motion using a fourth order Runge-Kutta-Nyström method. It should be noted that the basis for the following discussion is always the simulations without gravity and this may not always be stated. If results with gravity are presented and discussed, these will be denoted clearly *with gravity* or subscript *g*.

3.3 Data processing

Probe areas with a size of 4 mm *x* 4 mm were placed in the flow at streamwise positions 200, 300 and 400 mm with a cross-stream distance of 10 mm in order to monitor the flow, three such areas are shown in figure 1a). This selection leads to data similar to those of the Particle Image Velocimetry measurements of Hardalupas & Horender (2003a) and Horender & Hardalupas (2009). For each time step of the computation, the fluid velocity and the velocity of all particles present in that probe area were stored for further processing. These data were processed so that the mean and rms of fluid and particle velocity fluctuations were computed and the particle concentration was determined by counting the number of particles in the probe area at each time step. Each particle contributed to the computation of mean and rms of velocity fluctuations, regardless of how many particles were in the probe area. The covariances were evaluated according to

$$\left\langle u_f' u_p' \right\rangle_p = \left\langle \left(u_f(t)-U_f\right)\left(u_p(t)-U_p\right)\right\rangle_p \tag{11}$$

and in the same way for $\langle u'_p u'_f \rangle$ for each particle present in the probe area.

Statistical uncertainties for the particle and fluid velocities were 0.8% for the mean and 1.4% for the rms of the fluctuations and were the same for fluid and particle velocities, since all quantities were based on 10800 samples. The statistical uncertainties of the particle concentration were 2% for the mean and 1.4% for the rms of the fluctuations. The statistical uncertainties of the covariances varied with measurement position, since the number of contributing measurements depended on the mean particle concentration and varied between 300 and 2000. Hence, the statistical uncertainties were between 7% and 13% for the covariances seen by the particles.

4. Results

4.1 'Clean' shear layer flow

Figure 1a) shows the fluid flow structure as a contour plot of the streamwise fluid velocity while figure 1b) indicates the instantaneous positions of the computational vortices at the same time. Clearly, the pairing of the large vortices and the consequent growth of the shear flow can be observed. The positions of the particles are also shown and will be discussed below. Additionally, three probe areas with its original size of 4 mm times 4 mm are shown on figure 1a). At these positions, various spatially averaged particle characteristics were extracted and the corresponding probability density functions of fluctuating velocities will be presented below.

Figure 2 shows cross-stream profiles of the a) mean and b) variance of fluctuations of streamwise and cross-stream fluid velocities for streamwise positions x = 200, 300 and 400 mm. The cross-stream mean fluid velocity shows that fluid entrainment was captured by the model and in the streamwise mean velocity, a growth of the thickness of the shear layer was observed. The maximum intensity of streamwise velocity fluctuations normalised by the velocity difference across the shear layer was 21% and remained nearly constant with streamwise development. The intensity of the cross-stream velocity fluctuations was larger and increased with streamwise development, which is not consistent with experimental findings of, for example, Wygnanski & Fiedler (1970). This may be due to the fact that the model does not capture properly viscous effects, hence energy cannot be dissipated (Leonard 1980, p. 304), or due to the two-dimensionality, which does not allow vortex stretching as one of the main vortex interaction mechanisms in turbulent flows. However, the structure of a developing shear layer and the dispersion of particles is governed by these pairing large scale vortices, see for example the DNS calculations of Ling et al. (1998, fig. 21). Therefore, the results of the current two-dimensional calculations still can give valuable insight in the mechanisms of turbulence modification.

The production of turbulent kinetic energy p_{tke} was estimated as

$$p_{tke} = -2\left\langle u_f' v_f' \right\rangle \cdot \frac{dU_f}{dy} \tag{12}$$

leading to p_{tke} = 76, 51 and 38 m^2/s^2 on the centre line for streamwise positions 200, 300 and 400 mm. This quantity will also be used to normalise turbulence modification by the presence of particles, since the viscosity was not available due to the inviscid nature of the applied DVM, e.g. Hardalupas & Horender (2003a). As a consequence, the large scale Reynolds number cannot be defined straight forward as the ratio of velocity times dimension to viscosity. We had calculated the Reynolds number in our previous paper Hardalupas & Horender (2003a) as 1500, which is fairly low for a turbulent flow, but again, the computed flow shows the typical large scale pairing vortex structure. This estimation of *Re* was based on the computed velocity autocorrelation function for the streamwise velocity component and from that the Taylor time scale was estimated by fitting a parabola to time lag zero. Additionally the integral time scale was estimated and the Reynolds number derived according to

$$\mathrm{Re} \approx 15\left(\frac{t_{\mathrm{int}}}{t_{Taylor}}\right)^2 . \tag{13}$$

4.2 Particle phase characteristics

The instantaneous distributions of 90 and 55 μm particles are shown in figure 1 for the same instant of time and without gravity applied. The smaller particles showed a more defined spatial distribution, for example at position *x*=440 mm and *y*=0. This can be attributed to the Stokes number, which was between 1.7 and 1.0 for streamwise positions *x*=200, 300 and 400 mm. For the 90 μm particles the Stokes number was between 4.5 and 2.6, respectively. Hence, the smaller particles had a Stokes number closer to unity and therefore showed stronger degree of clustering. The probe areas of size 4 mm x 4 mm of figure 1 were used for extracting the particle data that are discussed below.

Figure 3 shows cross-stream profiles of the mean and rms of fluctuations of concentration of the 90 and 55 μm particles. It can be seen that, due to dispersion, the mean concentration profile flattens and become even bimodal with streamwise development. The profiles of the rms of particle concentration fluctuations showed similar shapes as the mean concentration and the ratio of *c`/C* increased from around 1.0 to 1.5 with streamwise position. Hence, preferential particle concentration increased with streamwise position and this increase was even larger for the 55 μm

particles, for which c'/C increased from 1.2 to 2.0. Again, this can be explained by the Stokes number of around unity for the smaller particles.

If gravity is applied, as in the real experiments of Hardalupas & Horender (2003a), it was shown in Horender (2002) that dispersion decreased and the bimodality of the mean particle concentration was less pronounced. This is also shown in figure 3 for streamwise position x=300 mm only and both particle sizes.

In Horender (2002) additional calculations including the initial velocities of the particles of 2.7 m/s in streamwise and 0.2 m/s in cross-stream direction were performed to compare the results with the actual experiments. These slight changes in the inlet particle velocities did hardly change the outcome for streamwise positions larger than x=200 mm. However, it was found that particle dispersion was over predicted by the current model, for example at x=300 mm by approximately 60% when compared to the corresponding experiments. This magnitude could be linked to the two-dimensional simulation and the over prediction of the fluid cross-stream fluid and particle velocity fluctuations. Feeding these values to the theory of diffusion by Taylor (1921), also a too large dispersion was obtained as observed in the current simulations.

Additionally, the bimodality of the mean concentration profiles, which was more pronounced for the 55 μm particles was attributed to the interaction of particles with Stokes number around unity with the pairing fluid vortices in Horender & Hardalupas (2009). There, a comparison between measurements and the current simulations with gravity has been presented. This comparison showed that the simulations predicted well the mean particle concentration for streamwise position x=200 mm, however over predicted the spreading for larger streamwise positions. The reason for that might be the two-dimensionality of the computation and the fact that the fluid velocity fluctuations of the cross-stream component were over predicted. However, it should be noted that the observed discrepancies between experiment and computation do not influence the purpose of the current paper.

Figure 4 shows the mean and rms of fluctuations of the streamwise and cross-stream velocity of the 90 and 55 μm particles. The particles were accelerated for all streamwise positions and it could be observed that the cross-stream mean velocities dispersed the particles outwards from the centre line of the shear flow. The levels of rms of velocity fluctuations were larger on the low speed (y>0) side compared to the high speed side, which was also observed in experiments of Hishida et al. (1992) and Hardalupas & Horender (2003a). The levels of velocity fluctuations were larger for the smaller particles, which may be linked to the larger mean velocity gradient, see figure 4c), compared to the

larger particles, see figure 4a). For both particle sizes the maximum rms of velocity fluctuations was smaller than for the fluid velocity fluctuations by approximately 30% for the streamwise and 60% for the cross-stream component, respectively. The effect of gravity was small on the mean and rms of fluctuations of streamwise particle velocities for both particles sizes. Therefore, the mean streamwise particle velocities are only presented for the larger particles in figure 4a). For the cross-stream component the downward drift is visible in fig. 4a. Here, the mean cross-stream velocity for the larger 90 μm particles was reduced by approximately 0.2 m/s on the (upper) low speed side. For the cross-stream velocity fluctuations an increase of nearly 50% was observed on the (upper) low speed side for the 90 μm particle, see figure 4b), while the streamwise velocity fluctuations were hardly affected. For the smaller 55 μm particles, this increase for the cross-stream velocity fluctuations was only a few percent and, hence, for clarity is not shown on the figure. It should be noted that the 90 μm particles achieved fluctuation levels of the cross-stream velocity component with gravity that equalled that of the smaller 55 μm particles without gravity. This behaviour of the larger particles may be linked to the larger degree of clustering for the larger particles when gravity is applied. If one compares the intensity of concentration fluctuations, defined as c'/C, it can be seen from figure 3a) and b) that for cross-stream position y=20 mm, c'/C was 1.3 for the case without gravity and approximately 2.0 for the case with gravity. This increased clustering can be observed in the equivalent particle distribution of figure 1 when gravity is present (Horender, 2002 – figs. 55 and 56).

Since gravity had little influence on the velocities of the 55 μm particles, further results with gravity will only be presented for the larger particle sizes.

4.3 Evaluation of fluctuating fluid velocities ‘seen’ by the particles

Figure 5 shows all the source terms of the fluid phase turbulent kinetic energy of eq. (3) for the 90 μm particles for streamwise positions x=200, 300 and 400 mm for streamwise and cross-stream velocities. Figure 6 shows the same data for the 55 μm particles.

Figures 5a) and 6a) show the fluid velocity fluctuations viewed by the particles and these were all smaller than the Eulerian fluid velocity fluctuations shown in figure 2b) for both velocity components and all streamwise positions. This effect was most pronounced close to the centreline of the flow around y=0 and for the smaller particles, which can be explained by dispersion due to the vortical flow structures, which led to preferential concentration of the particles. As a consequence, the particles do not see all regions within the fluid vortices.

Figures 5b) and 6b) show the covariance of fluid and particle velocities, which are approximately 30% of the fluid auto-covariance for the larger particles and around 50% for the smaller particles, since these follow better the fluid vortical structures. For the larger particles, the maximum values for both velocity components increased with streamwise development and were located close to the centreline at y=0. For the smaller particles this trend was different; the magnitude of the fluid-particle velocity covariance decreased with streamwise development and the maximum value was shifted towards the (upper) low speed side. Gravity had small influence on the fluid covariance velocity fluctuations for the cross-stream component, see figure 5a). The fluid-particle velocity covariance was slightly increased with gravity on the (upper) low speed side, since gravity plays a selective role, so that only particles that do follow instantaneous upward fluid velocities well are present at the low speed side. These particles may also be better correlated with the coherent fluid structure, when they 'fall' due to gravity at the lower side of the flow.

Figures 5c) and 6c) show the mean relative velocities, which have larger absolute values for the 90 μm particles due to their larger inertia and, hence, more persistent mean motion. For streamwise positions x=200 and 300 mm, the maximum values of the mean relative velocity were located at cross-stream positions around y=20 to 30 mm and the minimum at around y=-20 to -30 mm. For positions further away from the centre line, the absolute values tend to decrease again on the low speed (upper) side, because particles that have dispersed that far within such small streamwise development have already adopted the mean fluid flow. With gravity and for the larger particles, the drift velocity was smaller compared to the case without gravity by around 0.2 - 0.3 m/s and this difference reduced on the upper (low) speed side for y>30 mm.

Figures 5d) and 6d) show the drift velocity, corresponding to the covariance of the normalized particle concentration fluctuations and fluid velocity fluctuations in the tracer limit. For the largest streamwise position, the drift velocity was similar for both particle sizes, while, for the smallest streamwise positions, the absolute values were larger for the larger particles. For the 90 μm particles, the maximum value on the (upper) low speed side streamwise drift velocity decreased with streamwise development, while the cross-stream drift velocity increased. For the 55 μm particles, there was also an increase for the cross-stream drift velocity, while there was no clear trend for the streamwise component. On the low speed side (y<0), both components of the drift velocity were zero at y=-10 mm and for positions further away from the centre the streamwise drift velocity became positive again while the cross-stream component was negative. There, the cross-stream drift velocity for the smaller particles was nearly constant at around 0.1 to 0.2 m/s, while for the larger particles the cross-stream drift velocity decreased with streamwise development. For the

larger particles and in the presence of gravity, the cross-stream drift velocity increased on the upper (low) speed side. On the lower (high) speed side, where V_d was negative its value increased also but still remained negative.

In order to discuss in more detail the influence of the particle spatial distribution pattern on the fluid-particle correlated motion, the probability density functions of the fluid velocities seen by the particles will be examined below. This is important for dispersion models and carrier-phase turbulence modification, since the particles can only influence the viewed fluid velocity and vice-versa. If, for example, no particles are present at extreme velocity deviations from the mean, these may not be attenuated or enhanced. Figure 7 presents the Eulerian probability density function (PDF) of *u* and *v* fluid velocity fluctuations compared to the PDF viewed by the two particle size classes at cross-stream positions *y*=-20, 0 and 20 mm and at streamwise position *x*=300 mm. The PDFs are all normalized by their maximum value.

Figure 7 a) and b) shows the Eulerian fluid velocity PDFs at *y*=20 mm on the upper low speed side of the flow together with those seen by the two particle size classes. The Eulerian PDF of the cross-stream component, fig. 7 b), was approximately symmetric with a near Gaussian shape skewed towards upward velocities (from high speed to low speed side), which shows entrainment, see figure 2a). The streamwise component showed a PDF skewed towards lower fluid velocities. The PDFs of fluid velocity fluctuations viewed by the particles were narrower compared to the Eulerian PDF and this effect was stronger for the cross-stream component. This is due to the fact that particles did not penetrate the vortex cores, which can be seen at position *x*= 380 to 420 mm and *y*=20 mm of figure 1b), due to centrifuging effects. Nearly no particles were present there, but in this region the fluid showed its extreme cross-stream velocity events, hence the particles viewed reduced fluid velocity fluctuations, which may have important consequences on particle dispersion.

Both particle sizes viewed increased number of upward fluid events between 0 m/s to 1.5 m/s, compared to the Eulerian one, for the cross-stream velocity component. For the larger particles and the case with gravity this effect was even more pronounced. This shows that the particles were located preferentially in regions with upward (towards y>0) fluid velocities, see for example figure 1b) *y*=20 mm and *x*=290 mm, where particles were present in the upward (towards low speed side) moving part of the corresponding fluid structure. However, at *x*=360 mm hardly any particles were present in the region with downward fluid velocity, since they were centrifuged away from the centre up to around *y*=50 mm. For the larger particles and gravity applied, the picture slightly changed and there were nearly no particles present at cross-stream positions *y*>40 mm, see figure 3a). Hence, fewer particles see the downward fluid velocity, as seen consequently in figure 7b).

Figures 7 c) and d) show the PDFs on the centre line at y=0 and x=300 mm. It could be observed that the particles see reduced fluid velocity fluctuations, in agreement with the previous results. For the cross-stream component and for the smaller particles, with Stokes number close to unity, the difference of fluid velocities seen by particles and the Eulerian PDF was more pronounced and nearly symmetric with respect to the mean cross-stream velocity. The reason was again particle clustering between the vortex cores, with the consequence that the particles were not present at locations with extreme fluid velocity events, see figure 1. For the larger particles and the case with gravity, the cross-stream fluid velocities seen by particles were slightly reduced compared to the case without gravity.

Figures 7e) and f) present the PDFs at cross-stream position y=-20 mm on the (lower) high speed side. At this position in the flow the mean velocity gradient became smaller compared to the centre line, see figure 2a), and hence the Eulerian PDF for the streamwise component was close to Gaussian. The streamwise velocity fluctuations viewed by the particles were close to the Eulerian one and only few large fluid velocity events, i.e. around 7 m/s, were not seen by the particles. The Eulerian PDF of the cross-stream velocity component was still skewed towards negative, corresponding to outward dispersing, velocities. The cross-stream fluid velocity PDF viewed by the particles showed considerably more negative fluid velocity events, i.e. around -0.5m/s, but the particles did not see extreme downward velocities, i.e. smaller than -2 m/s and extreme upward velocities, i.e. around 2 m/s. The reason for that was that, for example at x=340 mm and y=-20, figure 1b), particles were present just in a region of increased downward fluid velocity. However there are no particles anymore at x=390 mm and y=-20 mm, where the fluid moves upward again. This happened due to particles centrifuging out of the vortex core. Therefore the particles did see less extreme upward fluid velocity events. Gravity reduced this effect, maybe because particles from the upper side continue to move downwards in such a region.

In summary, the discussion of the fluid-particle velocity correlation has shown that the particles view reduced fluid velocity fluctuations, which was evaluated by the PDFs of fluid velocity fluctuations and justified by the physics of the dispersion of particles due to coherent fluid vortices. Gravity changed the dispersion pattern, which led to reduction or enhancement of fluid velocity events seen by particles, depending on cross-stream position.

In the next section, the consequence of the fluid-particle correlated motion on turbulence modification of the carrier phase will be investigated.

4.4 Turbulent energy transfer

Figure 8 shows the dissipation due to the fluid-particle correlated motion for the 90 μm particles at streamwise positions x=200, 300 and 400 mm. The local mean particle concentration in eq. (3) was based on an overall mass loading of 12% as in the experiments of Hardalupas and Horender (2003a).

The resulting extra dissipation with gravity applied is only presented for streamwise position x=300 mm.

The *terms 1a* generally predict fluid turbulence reduction, see figures 8 and 9, since the velocity fluctuations of the particles were smaller than those of the fluid. The total reduction, which is the sum of the contributions of streamwise and cross-stream components, corresponded to a few percent of the fluid turbulence production due to shear, see eq. (12). *Terms 2a* predict fluid turbulence enhancement, which is however always balanced by *terms 1a*, so overall reduction dominates. In the presence of gravity, all the terms reduced by approximately 30%. This may be explained by the fact that fluid velocity fluctuations seen by particles were nearly unchanged, while the mean concentration shifted downward away from the flow region of maximum turbulent energy transfer. Since the terms in eq. (3) scale directly with the local mass loading, the energy transfer was reduced.

For the 55 μm particles, the turbulence modification is presented in figure 9. Generally, the predicted turbulence reduction is larger by nearly a factor of two compared to 90 μm particles. This occurs although the smaller particles see smaller velocity fluctuations of the fluid, see figures 5a) and 6a), but they have a smaller particle relaxation time τ_p. Hence, they exchange energy with the fluid at a larger rate. The larger fluid-particle velocity covariance, due to the better ability of the smaller particles to follow the flow, does not balance the reduced fluid velocity fluctuations seen by the particles. Hence, more energy from the fluid velocity fluctuations is supplied to the smaller particles.

Terms 2a show small levels of turbulence production which is maximum in the fluid shear region within the (upper) low speed side for the smallest streamwise position x=200 mm for both particle sizes. At this location, the particles move faster than the fluid flow and hence supply energy to the fluid velocity fluctuations due to their non-uniform distribution. For the 90 μm particles at x=200 mm and y=10 mm *term* $2a_u$ nearly balanced *term* $1a_u$, but this was not the case for the cross-stream terms. Only for the largest streamwise positions x=300 and 400 mm and the smaller particles, the cross-stream *term 2a* reduced turbulence. At the streamwise position of 400 mm, the value of the

Stokes number is the smallest relative to all investigated positions and equal to 1.0. Hence, we observe that for Stokes numbers larger than 1, *terms 2a* of eq. (3) would predict turbulence enhancement and reduce the attenuation effects of *terms 1a*.

Another interesting observation is that the reduction of fluid turbulence is always larger for the cross-stream component compared to the streamwise component for all positions and both particle sizes. This would generate an anisotropy in the flow, which was measured by Poelma et al. (2007) in a grid generated turbulent particle-laden water flow and by Hwang & Eaton (2006) in isotropic homogeneous air turbulence. They observed that the decay rate of the cross-stream velocity fluctuations was larger than that of the streamwise component. However, we note that there are some uncertainties in generalising this finding of production of anisotropy to real three dimensional flows, since, in our two dimensional calculation, the cross-stream velocity fluctuations were larger than that of the streamwise component.

The magnitude of turbulence modification relative to the dissipation rate of the fluid will be discussed now. It can be observed that the extra dissipation of fluid turbulence by the presence of the particles is close to the dissipation of the single phase fluid flow, which was of the order of 15 m^2/s^3 on the centreline, as reported in section 3. At x=200 mm and y=0, the turbulent production rate was 76 m^2/s^3. The extra dissipation due to the particles, which is the sum of all contributing terms was maximum for the 55 μm particles at x=200 mm and y=0 mm and had a value of approximately 5 m^2/s^3 for the current mass loading of 12%. This is one third of the fluid dissipation rate and suggests that our simplification using one-way coupled simulations might show already some uncertainties and not be applicable for larger particle loadings. It shows that the observed extra dissipation may have a considerable influence on the equilibrium level of turbulent kinetic energy, which is determined by production, dissipation and turbulent transport. In regions with small shear, say at y=50 mm and x=400 mm, the turbulence production is small but for both particle sizes considerable extra dissipation appears. Hence, the equilibrium turbulence level there may be considerably influenced by the particles. Hwang & Eaton (2006) measured fluid dissipation for the single phase fluid flow of 4.3 m^2/s^3 and extra dissipation due to particles with mass loading 0.23 of 3.1 m^2/s^3. These measurements indicated that the two values were nearly equal, as the current calculations do.

Hwang & Eaton (2006) commented that turbulence attenuation in their experiment may have been considerably larger than eq. (3) suggested. This may have happened due to larger instantaneous forces on the particles due to the unsteady flow field leading to considerable contributions of the Basset history force. Inspired by this statement, we investigated the effect of the instantaneous

Reynolds number on the particle drag and on *term 1a* of the model equation.

This results in

$$\Pi_{k,term1a} = -\frac{C}{\rho_f}\left(\left\langle \frac{1}{\tau_{p,c}} u'_{if} u'_{if} \right\rangle_p - \left\langle \frac{1}{\tau_{p,c}} u'_{if} u'_{ip} \right\rangle_p\right), \quad (14)$$

where $\tau_{p,c}$ is the corrected particle relaxation time and is defined in eq. 0. The resulting transfer of turbulent energy is also shown in figure 9 at position x=300 mm for the u component only. It could be observed that due to increased drag, since Re_p was approximately between 1 and 10, the overall turbulence attenuation increased by 50% on the centre line and by 20-30% at the positions with maximum turbulence attenuation. This leads to the conclusion that using the instantaneous drag coefficient leads to prediction of larger turbulence attenuation. Additionally, taking into account the unsteady flow around the particles, which are of the scale of the smallest turbulence eddies, may even further increase the drag coefficient and lead to even larger energy transfer and turbulence attenuation.

5. Discussion and comparison with the literature

Eq. (1) has been used widely in the literature for modelling and describing the modification of carrier phase turbulence, both in numerical and experimental work. However, there is no discussion on the ability of this model equation to predict the magnitude of turbulence modification due to the presence of particles. However, this equation is only valid for two continuum media rather than a fluid and a dispersed phase. Therefore, Vermorel et al. (2003) suggested eq. (3), which contained fluid velocities seen by the particles and this avoids the problem of undefined properties in eq. (1) for positions where no particles are present.

Gore & Crowe (1991) and Hetsroni (1988) and (1989) reviewed several experiments related to modification of carrier phase turbulence due to the presence of a disperse phase or bubbles in pipe flows and jets. From the available data they concluded that the ratio of particle diameter to turbulent length scale of the fluid l_f is the most appropriate parameter to correlate the increase or decrease of carrier phase turbulence with the addition of a second phase. They found that for $d_p/l_f>0.1$ carrier phase turbulence was increased and for $d_p/l_f<0.1$ carrier phase turbulence was reduced. However, this ratio was used only to determine whether the turbulence level was increased or decreased but not by how much. Crowe (2000) suggested a model without considering particle concentration fluctuations, which could describe carrier phase turbulence modification on the basis of the above

length scale ratio, which used volume averaging of the fluctuating quantities instead of time averaging, as it was done in order to derive eq. (1). Crowe (2000) applied the resulting model equation for carrier phase turbulence to a pipe flow and found that for d_p/l_f between 0.05 and 0.1 the sign of carrier phase turbulence modification changed.

Additionally, the above reviews showed that the particle Stokes number, which ranged from 0.1 to 10,000 in the considered experiments, was not appropriate to describe carrier phase turbulence enhancement or reduction. The experiments, which showed enhancement of carrier phase turbulence, all had either particle Stokes numbers above 200 or below 0.2 and included flows with solid particles or droplets and bubbles. Preferential particle concentration may not have appeared in these flows. However, the investigated flows with Stokes number around unity showed a large scatter in turbulence reduction between 0 and around 50%. The current simulations used 55 and 90 μm particles, while the length scale of the turbulent flow structures was similar to the shear layer width, which was 50 mm. Hence, d_p/l_f was approximately between 0.001 and 0.002. According to the reviewed experiments by Gore & Crowe (1991), this ratio should lead to turbulence reduction, since it was far below 0.1 and eq. (3) predicted this trend.

Schreck & Kleis (1993) - their figs 21 and 22 - compared the influence on the spectra of water velocity fluctuations due to plastic and glass beads with corresponding Stokes numbers of 1.9 and 3.5, based on Kolmogorov scale, while the sizes were equal. Hence the plastic beads follow better the dissipating eddies. They found that the plastic beads enhanced turbulence at large wave numbers in the Kolmogorov range, while the glass beads did not have an effect. It could be speculated that there is an effect, which increases the fluid turbulent velocity fluctuations, for example due to the wakes of the particles. It could be that *term 1a* leads to a reduction of fluid turbulence due to fluid-particle correlated motion, which balances the (unknown) production effect. For the lighter plastic beads *term 1a* would predict smaller turbulence reduction, since these follow the flow better and, therefore, overall augmentation was found.

Kulick et al. (1994) measured turbulence modulation in a particle-laden pipe flow for a range of particle Stokes numbers 0.6 (50 μm glass beads) to 3 (70 μm copper particles). They found carrier phase turbulence reduction for the copper particles of around 26% on the centre line of the pipe for mass loading 20%. However, for the glass beads with the same mass loading, carrier phase turbulence modification was negligible. In Fessler et al. (1994), they used exactly the same flow with Kolmogorov length scale 190 μm. They found that the glass beads showed preferential concentration on the Kolmogorov scale, while the distribution of the copper particles was close to randomness. Hence, one reason for the different behaviour of the two particle size classes in Kulick

et al. (1994) could be particle clustering. Therefore, the 50 μm glass beads in their experiments could have had a very small effect on carrier phase turbulence, since they see smaller fluid velocity fluctuations and together with that are better correlated with the fluid velocity fluctuations, hence the results of eq. (3) may be small. In contrast to that, their 70 μm copper particles did not show preferential concentration, hence viewed larger fluid velocity fluctuations and were less correlated with the fluid velocity fluctuations, hence eq. (3) would predict turbulence reduction. This trend, for the current flow, has been shown in figures 5a) and 6a) for the fluid velocities viewed by the particles.

Fessler & Eaton (1999) measured turbulence modification in a backward facing step flow laden with 90 and 150 μm glass beads and 70 μm copper particles, with Stokes numbers 3.0, 7.2 and 6.9 and particle Reynolds numbers of 7.3, 11.8 and 5.5 respectively. The Kolmogorov scale was estimated as 170 μm on the centre line. They found that the reduction of gas phase turbulence was an increasing function of the particle Stokes and Reynolds number and could reach up to 35 % of the clean flow level at a mass loading of 40 %. They argued that an increase of particle Reynolds number could lead to turbulence enhancement due to streamline distortion of the carrier fluid. They showed that a simplified version of eq. (1) would predict an opposing trend. However, our results indicate that the fluid-particle correlated motion together with preferential concentration may strongly influence the outcome of the model equation, hence the results of such simplified forms of eqs. (1) or (3) may not be realistic. In addition, the flow regime was found to strongly affect the degree of turbulence modification. After the reattachment point of the recirculating region behind the step, very little turbulence modification was observed, although the number density of particles was as high as in the channel flow extension, where significant modification was found. They concluded that the flow structure in the shear region did not allow the particles to modify the gas flow turbulence levels. However, this is the region where particle clustering may be expected and one reason for the observed negligible turbulence modification could again be due to balancing out the opposing effects of *terms 1a* and *2a* of eq.(3).

Yang & Shy (2005) observed turbulence production at the Kolmogorov scales for all flow conditions together with particle clustering. Although they did not quantify preferential concentration, their study shows experimentally that *term 2a* may have the ability to model turbulence production.

6. Conclusions

This paper presented the balance of the terms contained in the model equation for carrier phase turbulence modification by the presence of solid particles including the effect of preferential particle concentration. For this evaluation, a particle-laden shear layer with Stokes numbers 1.0 to 4.5 was simulated by a two-dimensional discrete vortex method with one-way coupling. Therefore, the presented results are valid for dilute flows where the particle influence on the flow scales linearly with their loading.

The results were analysed in terms of the averaged fluid velocity characteristics seen by the particles and corresponding velocity PDFs. It has been shown that the viewed PDFs of fluid velocity fluctuations seen by particles become asymmetric and even bimodal due to the coherent vortical structures of the flow. Additionally, the particles viewed reduced fluid velocity fluctuations when compared to the Eulerian fluid velocity PDFs, as a consequence of the resulting preferential particle concentration patterns occurring due to the interaction with the two-dimensional fluid flow large scale vortices.

The results of the model for carrier phase turbulence modification indicated carrier phase turbulence attenuation, which was linked with the fluid-particle correlated motion. The magnitude of extra dissipation could reach values of one third of the single phase fluid dissipation in the currently studied two-dimensional shear flow and was larger for the smaller particles. Preferential particle concentration together with a relative velocity between the phases could lead to turbulence enhancement, however this magnitude was always smaller than the turbulence attenuation in our test case. These findings in a two-dimensional flow were considered in the context of available experiments in the literature considering real three-dimensional turbulent flows, which allowed an improved discussion and a separation of different effects leading to turbulence reduction and augmentation.

Additionally, the Reynolds number dependence of the instantaneous drag coefficient was taken into account by using a corrected particle relaxation time in the model for turbulence modification. This resulted in a carrier phase turbulence attenuation increased by a factor of 1.3 to 1.5 for both particle sizes compared to the model evaluation using the Stokes drag coefficient. Hence, future work should use Reynolds number corrections for the drag based on the instantaneous slip velocity to evaluate energy transfer in dispersed phase flows.

Acknowledgements

SH would like to thank the Institute of Fluid Mechanics of the German Aerospace Research Centre (DLR) in Göttingen for funding during the development of the numerical code. Partial support from Engineering Physical Sciences Research Council (EPSRC) through grant GR/N04553 is acknowledged.

References

Bini, M., Jones W.P., 2008. Large-eddy simulation of particle-laden turbulent flows. J. Fluid Mech. 614, 207-252.

Boivin, M., Simonin, O., Squires, K.D., 1998. Direct numerical simulation of turbulence modulation by particles in isotropic turbulence. J. Fluid Mech. 375, 235-263.

Brown, G.L., Roshko, A., 1974. On density effects and large structure in turbulent mixing layers. J. Fluid Mech. 64, 775-816.

Chang, K.C., Wang, M.R., Wu, W.J., Liu, Y.C., 1993. Theoretical and Experimental Study on Two-Phase Structure of Plane Mixing Layer. AIAA Journal 31 no.1, 68-74.

Chein, R., Chung, J.N. 1988. Simulation of Particle Dispersion in a Two-Dimensional Mixing Layer. AIChE Journal 34, 946-954.

Chen, C.P., Wood, P.E., 1985. A Turbulence Closure Model for Dilute Gas-Particle Flows. Canadian J. Chem. Eng 63, 349-360.

Chorin, A.J, 1973. Numerical Study of Slightly Viscous Flow. J. Fluid Mech. 57, 785-796.

Chung, J.N., Troutt, T.R., 1988. Simulation of particle dispersion in an axisymmetric jet. J. Fluid Mech. 186, 199-222.

Cottet, G.-H., Koumoutsakos, P.D., 2000. Vortex Methods: Theory and Practice. Cambridge University Press.

Crowe, C.T., 2000. On models for turbulence modulation in fluid-particle flows. Int. J. Multiphase Flow 26. 719-727.

Crowe, C.T., Gore, R.A., Troutt, T.R., 1985. Particle dispersion by coherent structures in free shear flows. Part. Sci. Technol. J. 3, 149-158.

Crowe, C.T., Chung, J.N., Troutt, T.R., 1993. Particle Dispersion by Organized Turbulent Structures. In: Roco MC (ed) Particulate Two-Phase Flow, 626-669.

Eaton, J.K., Fessler, J.R., 1994. Preferential Concentration of Particles by Turbulence. Int. J. Multiphase Flow 20, 169-209.

Elghobashi, S., Abou-Arab, T.W., 1983. A two-equation turbulence model for two-phase flows, Phys. Fluids 26, 931-938.

Elghobashi, S., Truesdell, G.C., 1993. On the two-way interaction between homogeneous turbulence and dispersed solid particles. I: Turbulence modification. Phys. Fluids A 5, 1790-1801.

Fessler, J.R., Eaton, J.K., 1999. Turbulence modification by particles in a backward-facing step flow. J. Fluid Mech. 394, 97-117.

Fessler, J.R., Kulick, J.D., Eaton, J.K., 1994. Preferential concentration of heavy particles in a turbulent channel flow. Phys. Fluids 6, no. 11, 3742-3749.

Geiss, S., Dreizler, A., Stojanovic, Z., Chrigui, M., Sadiki, A., Janicka, J., 2004. Investigation of turbulence modification in a non-reactive two-phase flow. Exp. Fluids 36, 344-354.

Gore, R.A., Crowe, C.T., 1991. Modulation of turbulence by dispersed phase. J. Fluids Engineering 113, 304-307.

Hagiwara, Y., Murata, T., Tanaka, M., Fukawa, T., 2002. Turbulence modification by the clusters of settling particles in turbulent water flow in a horizontal duct, Powder Technology 125, 158-167.

Hardalupas, Y,. Horender, S., 2003a. Fluctuations of particle concentration in a turbulent two-phase shear layer. Int. J Multiphase Flow 29, 1645-1667.

Hardalupas, Y,. Horender, S., 2003b. A method to estimate gas-droplet velocity cross-correlations in sprays, Atomization and Sprays 13, 273-295.

Hetsroni, G., 1988. Particles-Turbulence Interaction. Invited Lecture ASME Winter Annual Meeting. Chicago. Illinois.

Hetsroni, G., 1989. Particles-turbulence interaction. Int. J. Multiphase Flow 15, 735-746.

Hishida, K., Ando, A., Maeda, M., 1992. Experiments on Particle Dispersion in a Turbulent Mixing Layer. Int. J. Multiphase Flow 18, no. 2, 181-194.

Horender, S., 2002. Experiments and Simulations of Particle-laden Turbulent Shear Flows. PhD Thesis. Imperial College. London. UK.

Horender, S., Hardalupas, Y., 2009. Turbulent particle mass flux in a two-phase shear flow. Powder Technology 192, 203-216.

Horender, S., Lipowsky, J., Schwerin, M., Badeke, K.U., Sommerfeld, M., 2008. Deposition of SiO_2 nanoparticles produced in a turbulent H_2/O_2 flame. Aerosol Sci. Tech. 42, 873-883.

Huang, Y., Wu, W., Zhang, H., 2006. Numerical study of particle dispersion in the wake of gas particle flows past a circular cylinder using the discrete vortex method. Powder Technology 162, 73-81.

Hwang, W., Eaton, J.K., 2006. Homogeneous and isotropic turbulence modulation by small heavy (St~50) particles. J. Fluid Mech. 564, 361-393.

Hädrich, T., 2001. Measurement of turbulent spectra of particle-laden flows in a horizontal channel, Exp. Fluids 31, 401-408.

Kulick, J.D., Fessler, J.R., Eaton, J.K., 1994. Particle response and turbulence modification in fully developed channel flow. J. Fluid Mech. 277, 109-134.

Kussin, J., Sommerfeld, M., 2002. Experimental studies on particle behaviour and turbulence modification in horizontal channel flow with different wall roughness, Exp. Fluids 33, 143-159.

Lázaro, B.J., Lasheras, J.C., 1992. Particle dispersion in the developing free shear layer. Part 1. Unforced Flow. J. Fluid. Mech 235, 143- 178.

Leonard, A., 1980. Vortex methods for flow simulations. J. Comp. Phys. 37, 289-335.

Leonard, A., 1985. Computing Three-Dimensional Incompressible Flows with Vortex Elements. Ann. Rev. Fluid Mech. 17, 523-559.

Ling, W., Chung, J.N., Troutt, T.R., Crowe, C.T., 1998. Direct numerical simulation of a three-dimensional temporal mixing layer with particle dispersion. J. Fluid Mech. 358, 61-85.

Ljus, C., Johannsson, B., Almstedt, A.-E., 2002. Turbulence modification by particles in a horizontal pipe flow, Int. J. Multiphase Flow 28, 1075-1090.

Longmire, E.K., Eaton, J.K., 1992. Structure of a particle-laden round jet. J. Fluid Mech. 236, 217-257.

Melheim, J.A., Horender, S., Sommerfeld, M., 2005. Modeling of the Vortex-Structure in a Particle-laden Mixing-Layer, FEDSM2005-77040, ASME Fluid Eng. Division Summer Meeting & Exhib., Houston.

Poelma., C., Westerweel, J., Ooms, G., 2007. Particle-fluid interactions in grid-generated turbulence. J. Fluid Mech. 589, 315-351.

Pope, S.B., 2000, Turbulent Flows, Cambridge University Press.

Reeks, M.W., 1993. On the constitutive relations for dispersed particles in nonuniform flows. I: Dispersion in a simple shear flow. Phys. Fluids A 5, 750-761.

Sarpkaya, T., 1989. Computational methods with vortices – The 1988 Freeman Scholar Lecture. J. Fluids Eng. 111, 5-52.

Schreck, S., Kleis, S.J., 1993. Modification of grid-generated turbulence by solid particles, J. Fluid Mech. 249, 665-688.

Simonin, O., Deutsch, E., Minier, J.P., 1993. Eulerian prediction of fluid/particle correlated motion in turbulent two-phase flows. Appl. Sci. Res. 51, 275-283.

Taylor, G.I., 1921. Diffusion by continuous movements, Proc. Lond. Math. Soc., Vol. 20, 196-212.

Ten Cate, A., Derksen, J.J., Portela, L.M., van den Akker, H.E.A., 2004. Fully resolved simulations of colliding monodisperse spheres in forced isotropic turbulence, J. Fluid Mech. 519, 233-271.

Uchiyama, T., Naruse, M., 2006. Numerical simulation of reacting plane mixing layer by particle method, Chem. Eng. Sci. 61, 7299-7308.

Vermorel, O., Bédat, B., Simonin, O., Poinsot, T., 2003. Numerical study and modelling of turbulence modulation in a particle laden slab flow, J. of Turbulence 4, 1-39.

Wen, F., Kamalu, N., Chung, J.N., Crowe, C.T., Troutt, T.R., 1992. Particle Dispersion by Vortex Structures in Plane Mixing Layers. J. Fluids Engineering 114, 657-666.

Winant, C.D., Browand, F.K., 1974. Vortex pairing, the mechanism of turbulent mixing layer growth at moderate Reynolds numbers. J. Fluid Mech. 63, 237-255.

Wygnanski, I., Fiedler, H.E., 1970. The two-dimensional mixing region. J. Fluid Mech. 41, 327-362.

Yang, T.S., Shy, S.S., 2005. Two-way interaction between solid particles and homogeneous air turbulence: particle settling rate and turbulence modification measurements, J. Fluid Mech. 526, 171-216.

Figures

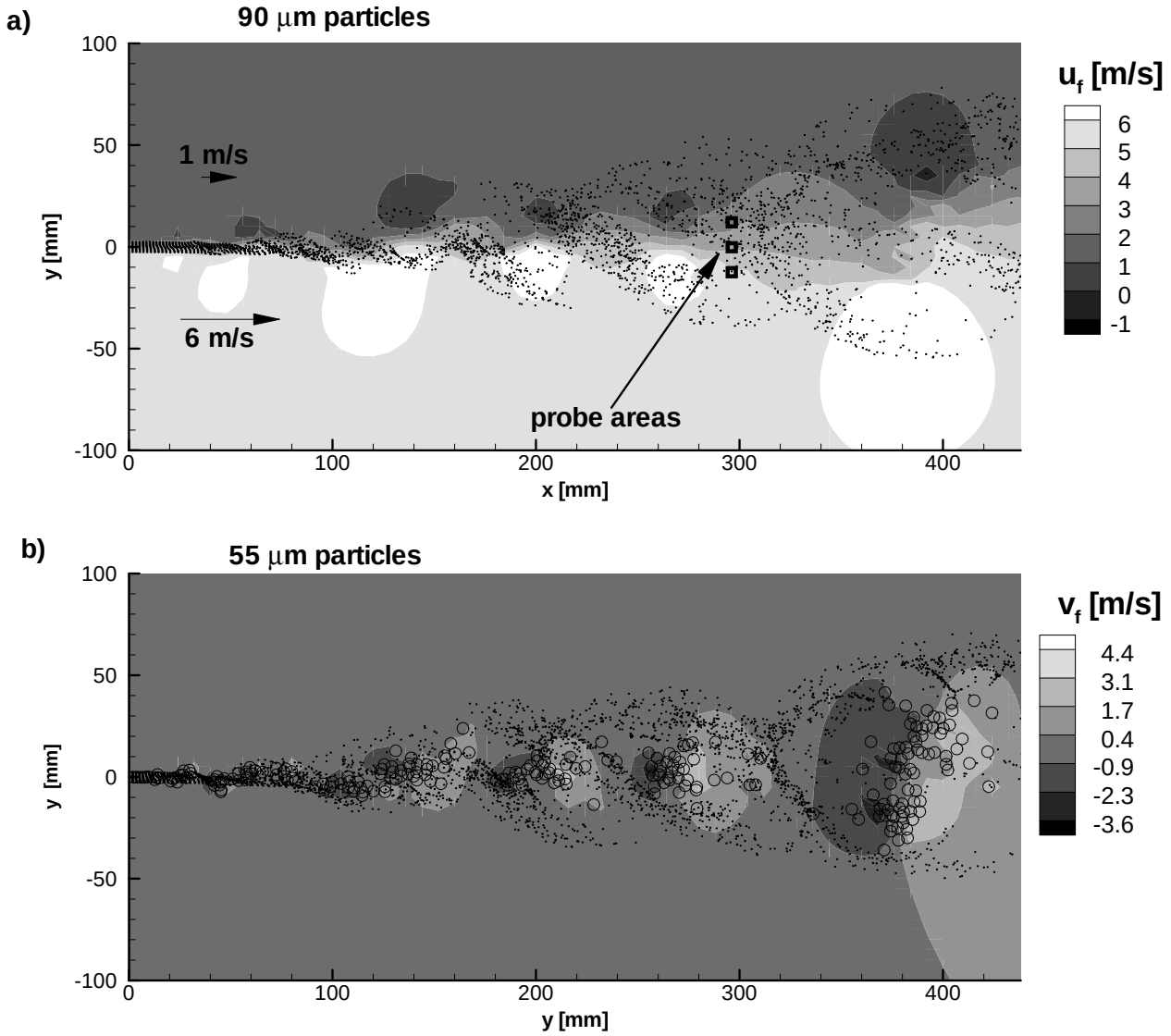

Figure 1. Flow configuration: a) contour plot of instantaneous streamwise fluid velocities and particle positions for 90 μm particles, b) contour plot of instantaneous cross-stream fluid velocities and 55 μm particles and the computational vortices at the same instant of time; points are the particles, hollow circles represent the computational vortices. Boxes indicate position of velocity PDFs shown in fig. 7.

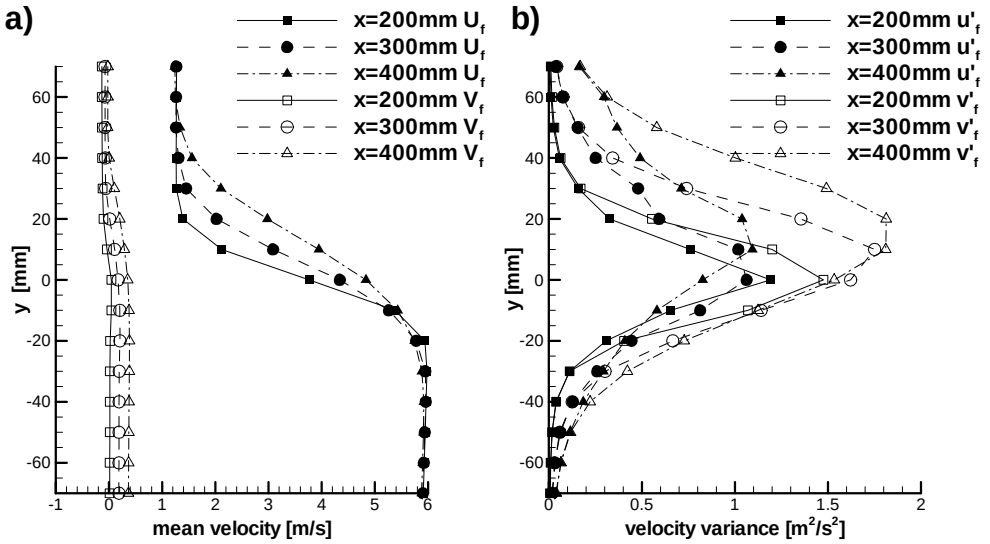

Figure 2. Cross-stream profiles of the a) mean and b) variance of streamwise and cross-stream velocity fluctuations of the fluid for streamwise positions x = 200, 300, 400 mm.

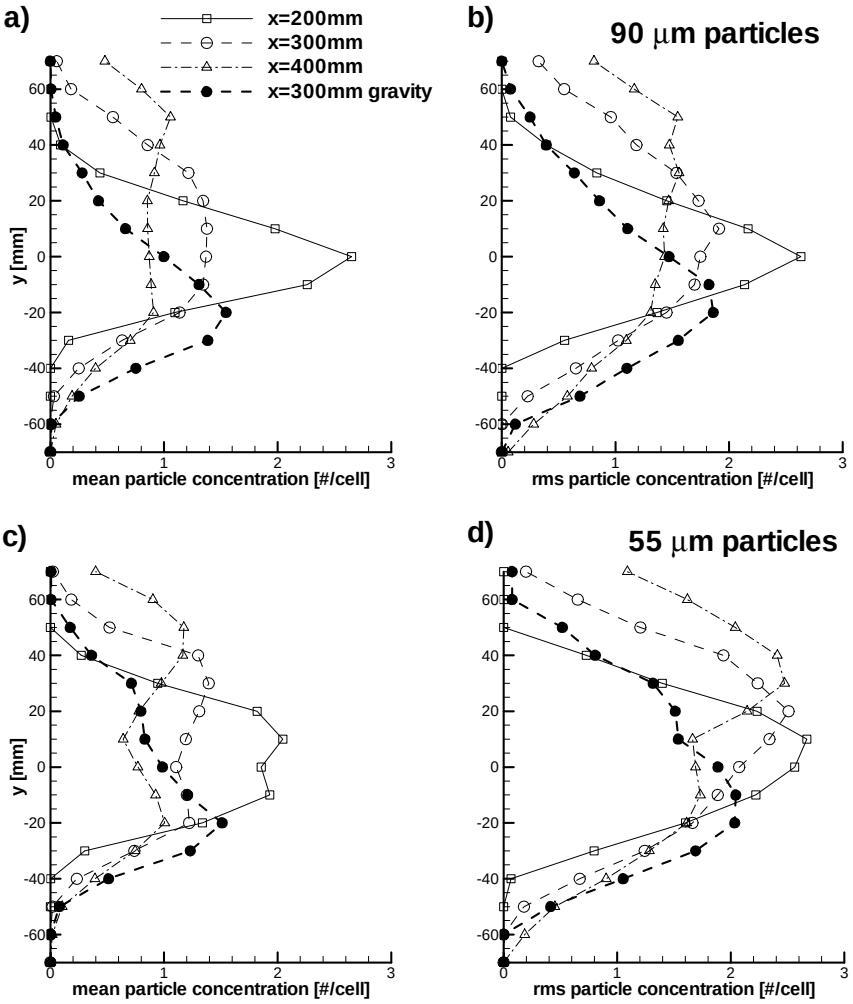

Figure 3. Cross-stream profiles of a) mean and b) rms of particle concentration for 90 μm particles

for streamwise positions x = 200, 300, 400 mm. c) and d) same data for 55 μm particles.

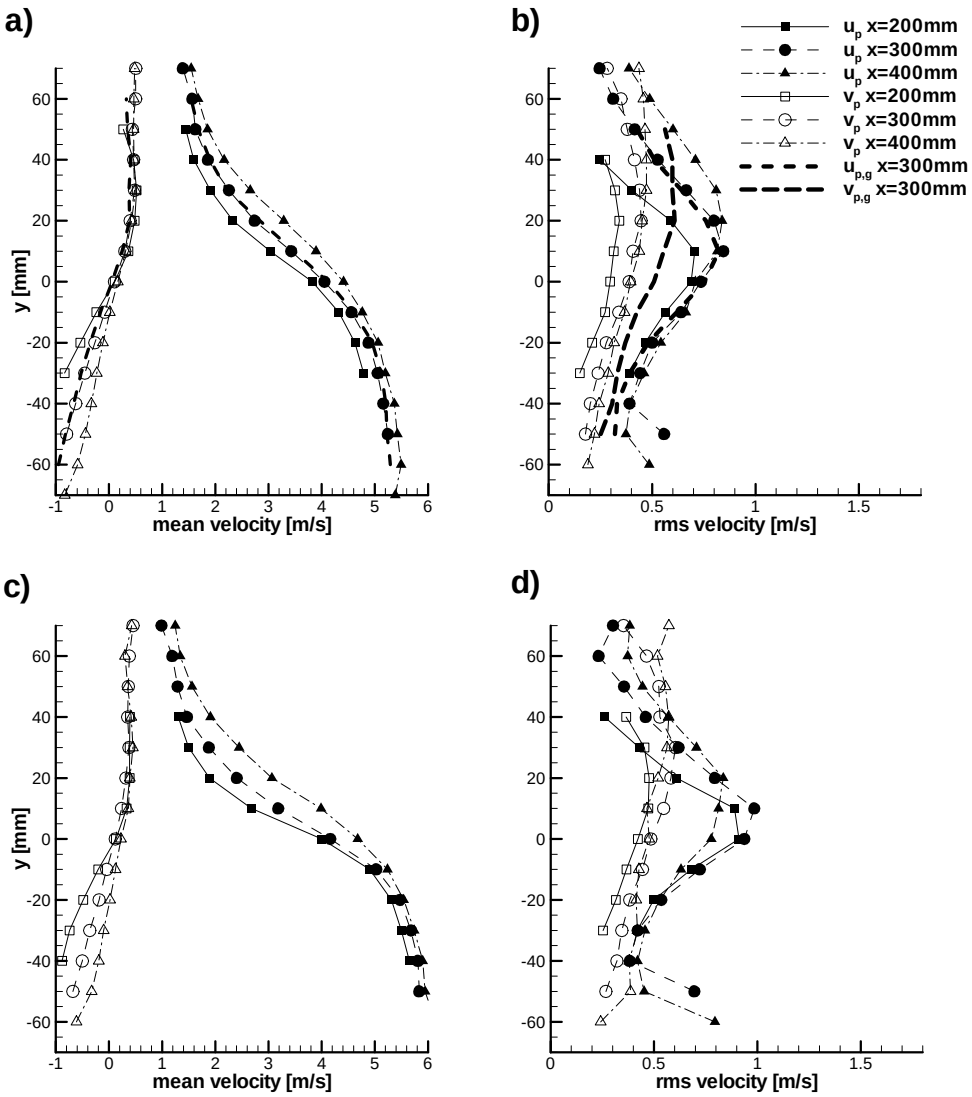

Figure 4. a) Mean and b) rms streamwise and cross-stream particle velocities for 90 μm particles. c) and d) same data for 55 μm particles. Full symbols denote streamwise and hollow symbols cross-stream components.

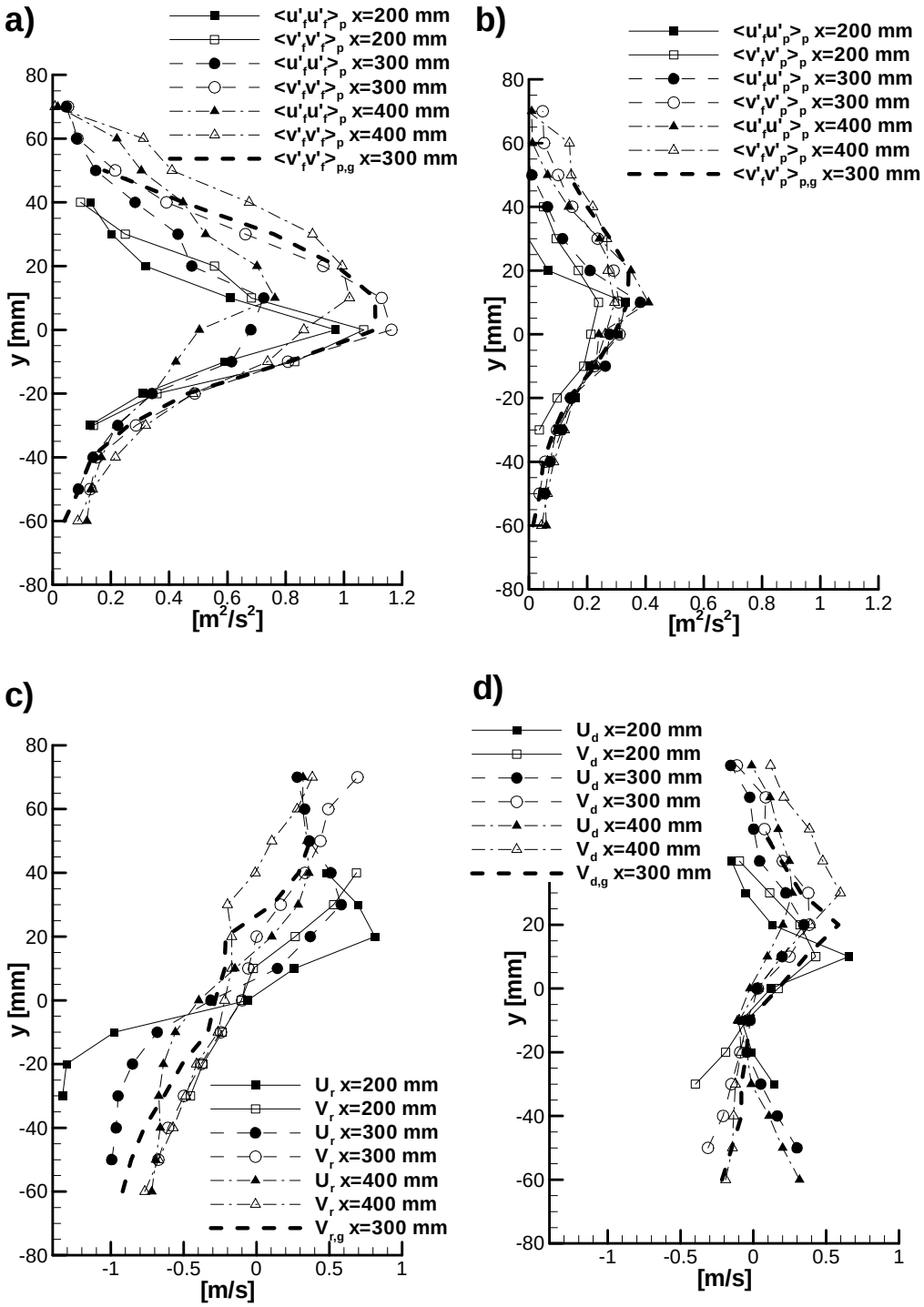

Figure 5. Cross-stream profiles of fluid velocity statistics viewed by the 90 μm particles. a) covariance of fluid velocity fluctuations $\langle u'_{if}\, u'_{if}\rangle$, b) covariance of fluid and particle velocity fluctuations $\langle u'_{if}\, u'_{ip}\rangle$, c) relative velocity $U_{ir}=\langle u_{ip}-u_{if}\rangle_p$ between fluid and particles and d) drift velocity $U_{id}=\langle u'_{if}\rangle_p$.

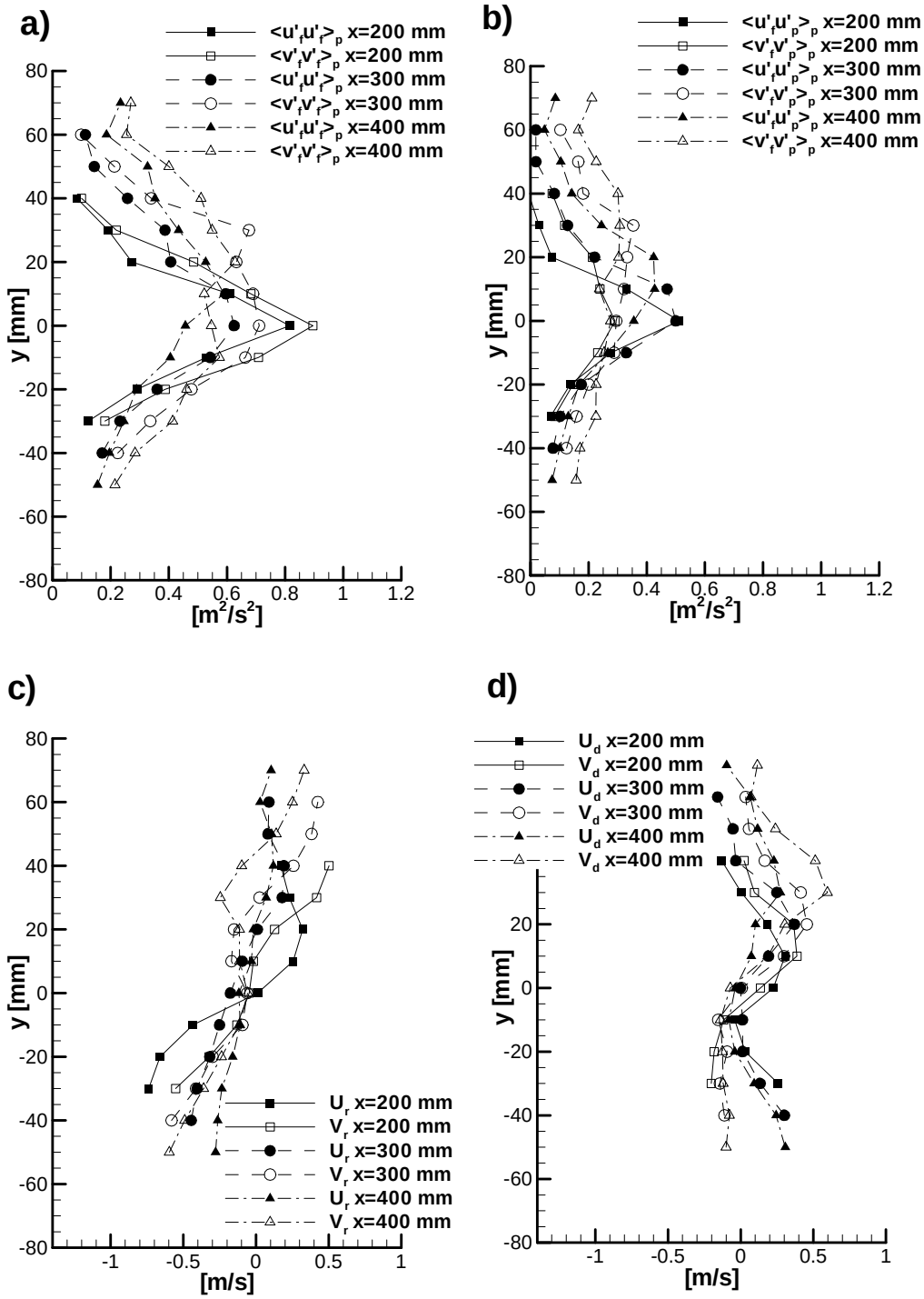

Figure 6. Cross-stream profiles of fluid velocity statistics viewed by the 55 μm particles. a) covariance of fluid velocity fluctuations $\langle u'_{if}\, u'_{if}\rangle$, b) covariance of fluid and particle velocity fluctuations $\langle u'_{if}\, u'_{ip}\rangle$, c) relative velocity $U_{ir}=\langle u_{ip}-u_{if}\rangle_p$ between fluid and particles and d) drift velocity $U_{id}=\langle u'_{if}\rangle_p$.

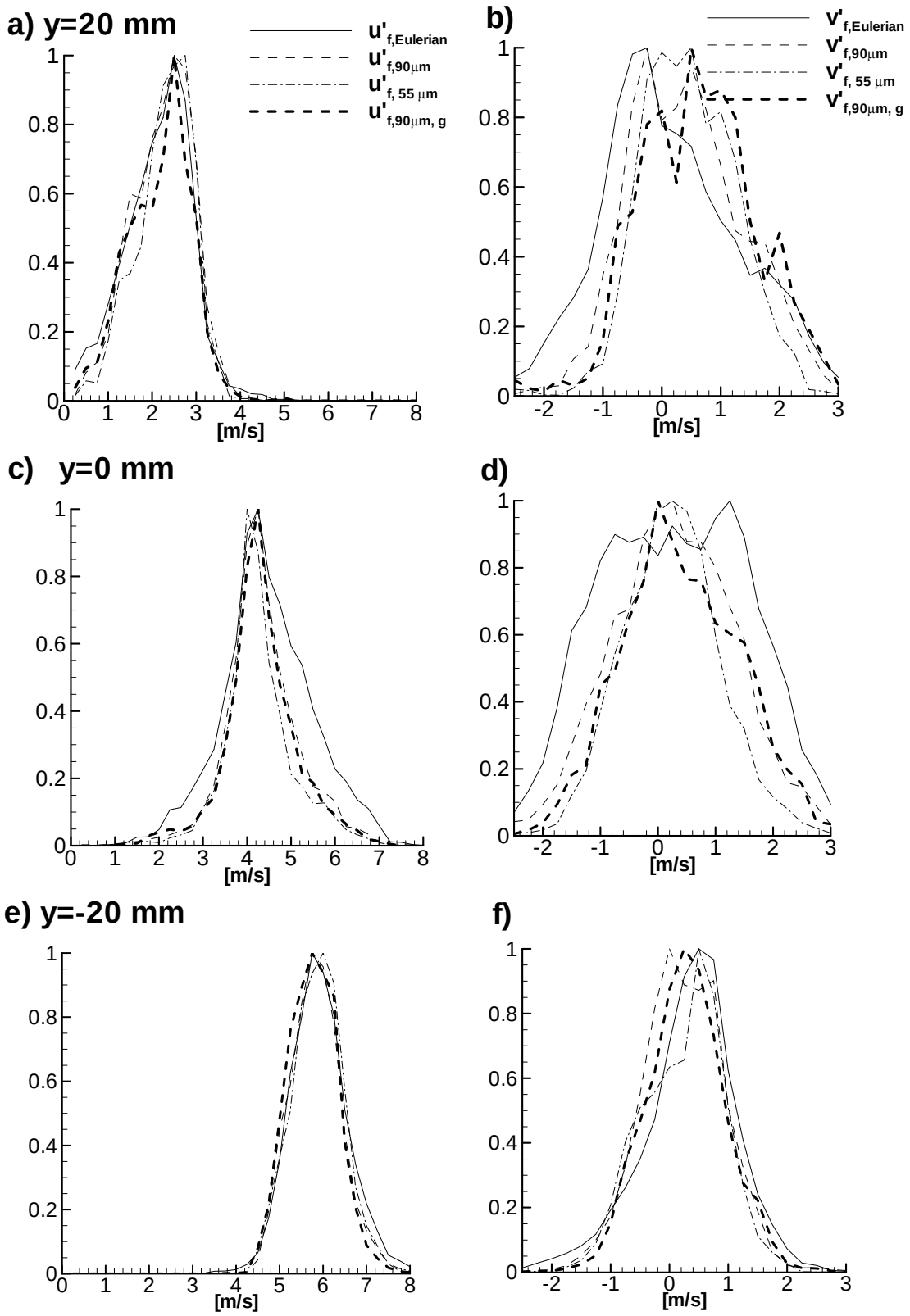

Figure 7. PDF of Eulerian fluid velocity fluctuations at fixed position, and as seen by the 90 and 55 μm particles at streamwise position x=300 mm for cross-stream positions y=20, 0 and -20 mm. a), c) and e) streamwise component, b), d) and f) cross-stream component.

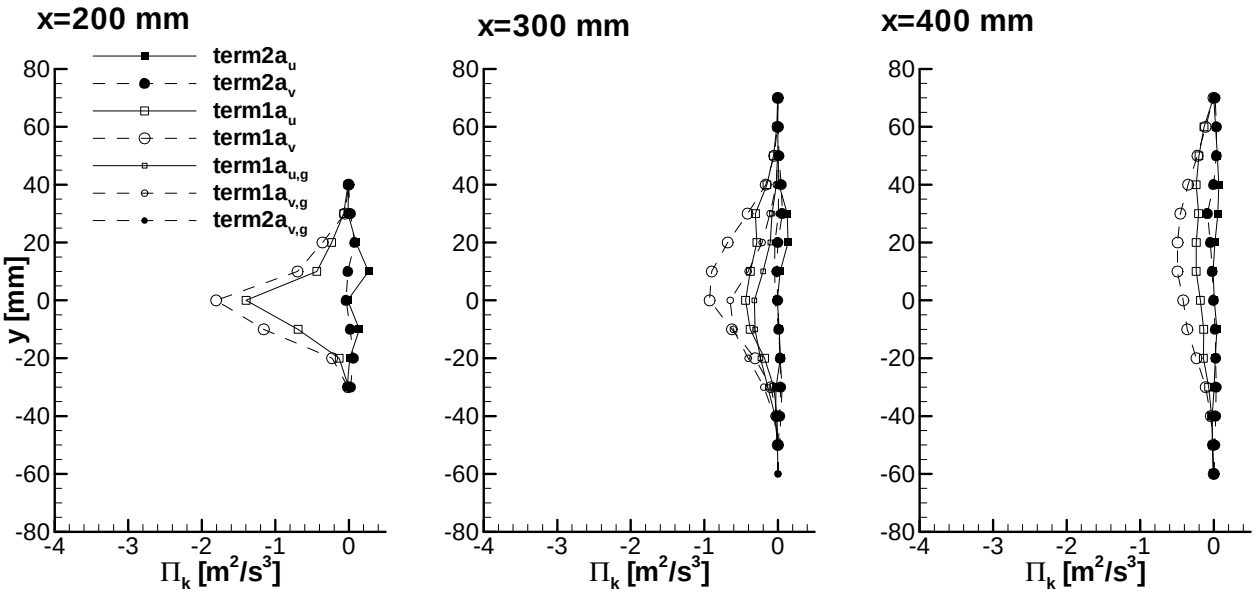

Figure 8. Fluid turbulence modification terms according to eq. (3) due to the 90 μm particles for streamwise positions *x*=200,300 and 400 mm.

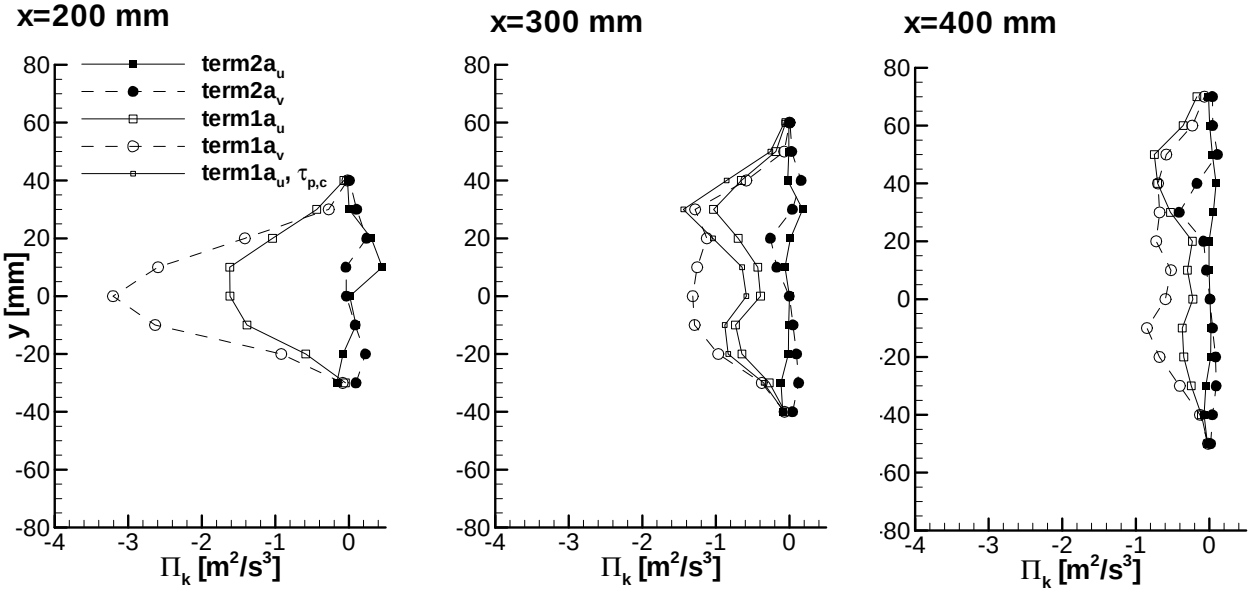

Figure 9. Fluid turbulence modification terms according to eq. (3) due to the 55 μm particles for streamwise positions *x*=200,300 and 400 mm; additionally at *x*=300 mm the influence of the corrected particle relaxation time based on eq. (14) is shown.